Mar Geophys Res (2012) 33:289–305
DOI 10.1007/s11001-012-9149-1

ORIGINAL RESEARCH PAPER

Multiple attenuation in crustal-scale imaging: examples from the TAIGER marine reflection data set

Ryan Lester · Kirk McIntosh

Received: 31 March 2011 / Accepted: 16 March 2012 / Published online: 15 April 2012

Abstract During summer of 2009, multi-channel marine seismic reflection data and wide-angle refraction data were acquired as part of the joint NSF and Taiwanese-funded TAIGER program with the goal of understanding the dynamics of arc-continent collision in Taiwan. One of the principle difficulties of crustal-scale imaging with marine reflection data such as these is the prevalent multiple contamination that obscures many of the deep crustal targets. Without effective treatment of multiples, many of the objectives of the TAIGER active source program may not be achieved. We present three profiles, one from each acquisition leg, that demonstrate the effectiveness of 2D surface-related multiple elimination (SRME) and radon filtering in attenuating much of this unwanted energy in broad ranges of water depths, seafloor topographies and lithologies. Two profiles from south of Taiwan image 3–4 km of sedimentary strata overlying moderately extended continental crust along the Eurasia continental shelf and a 5–6 km thick sedimentary section overlying thin crust consisting of faulted blocks and volcanic bodies along the continental slope. Our multiple attenuation efforts also reveal a seaward-dipping normal fault that penetrates into the upper mantle and separates thick crust of the continental shelf from thin crust of the continental slope. A profile from east of Taiwan reveals thin ocean crust of the Philippine Sea plate subducting beneath the Ryukyu trench that may be traced beneath the accretionary prism and Ryukyu forearc. These profiles demonstrate the success of our imaging strategy in the range of imaging environments spanned by the TAIGER marine reflection seismic data.

R. Lester (✉) · K. McIntosh
Institute for Geophysics, University of Texas, Austin, TX, USA
e-mail: rlester@utexas.edu

Keywords Continental margin · Subduction zone · Crustal structure · Marine geophysics · Taiwan

Introduction

Taiwan was created when the southern Eurasia continental margin began colliding with the Luzon arc in the late Miocene. As one of only a handful of young, active arc-continent collisions, Taiwan has been the subject of many geologic investigations aimed at understanding the dynamics of arc-continent collision. As a consequence, many models have been developed here that have been applied not only to Taiwan, but to other mountain belts around the world (Davis et al. 1983; Wu et al. 1997). These models propose a spectrum of crustal and lithospheric behaviors during collision that have not been tested due to a lack of high-resolution crustal-scale geophysical constraints. During the summer of 2009, over 10,000 km of 2D marine seismic reflection data were acquired as part of the joint NSF and Taiwanese-funded TAIGER program with the goal of testing and refining hypothesized models of arc-continent collision (Fig. 1). These data, along with wide-angle seismic data recorded by OBS and land instruments, were acquired in a wide range of marine imaging environments with the goal of constraining different aspects of the orogen, as well as Eurasia continental margin southwest of Taiwan, Manila subduction system south of Taiwan and Ryukyu subduction system east of Taiwan—systems that impact the dynamics of the Taiwan arc-continent collision.

The TAIGER active source seismic program was designed to acquire data along different spatial transects that may represent different stages of collision. In particular, multi-channel seismic reflection data were acquired offshore southern Taiwan to image the incipient collision,

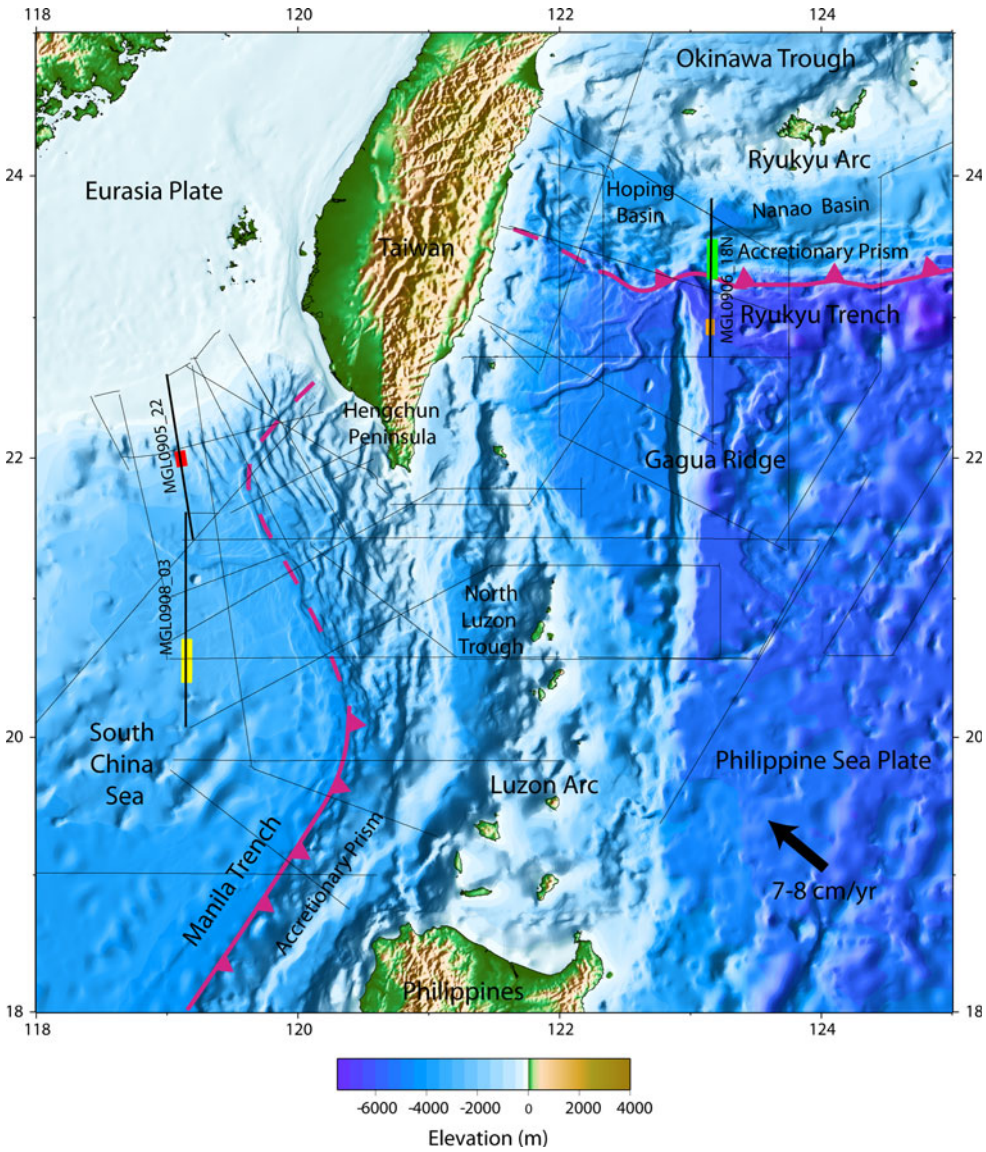

Fig. 1 Bathymetry map of Taiwan region with major tectonic features labeled. Convergence rate between Philippine Sea plate and Eurasia plate is 7–8 cm/year in a northwesterly direction. *Thin black lines* indicate marine reflection profiles acquired during the 2009 TAIGER active source program. *Thick black lines* are seismic profiles MGL0905_22, MGL0908_03, and MGL0906_18N discussed in this study. *Red box* is the section in Fig. 3, *orange box* is Fig. 4, *yellow box* is Figs. 6 and 8, and *green box* is Figs. 7 and 9

as well as the Eurasia continental margin and Manila trench subduction system south of the collision. The goal of imaging the Eurasia continental margin and Manila subduction system (i.e. accretionary prism, Luzon arc, forearc basin) is to delineate the crustal structure and materials thought to be similar to those involved in the collision. Similarly, multi-channel seismic reflection profiles were acquired east of Taiwan in the Philippine Sea to image the offshore extent of collision-related deformation and the Ryukyu subduction system, where the Philippine Sea plate is subducting northward adjacent to the Taiwan arc-continent collision. While the Eurasia continental margin, Manila and Ryukyu subduction systems merit study in their own right, the purpose of imaging these systems for the TAIGER project is to delineate the evolution of arc-continent collisions from the initial pre-collision stage, as represented by the Eurasia continental margin and Manila subduction system south of Taiwan, to the post-collision stage near the intersection of Taiwan and the Ryukyu trench.

There is a wide range of imaging targets within such an extensive dataset, including relatively flat strata of the Eurasian continental margin and abyssal plane, highly deformed sedimentary rocks of the Manila trench and Ryukyu trench accretionary prisms, and deep crystalline crustal structure, each with their own imaging challenges. Attenuation of multiples is one of the most ubiquitous of these challenges, and one of the primary challenges of any marine seismic reflection data set. Multiples are particularly problematic in crustal-scale imaging, as they often obscure reflections from deep imaging targets. The TAIGER reflection data span a variety of water depths, seafloor topographies, and lithologies, making the effective attenuation of all multiples an arduous task. The purpose of this

paper is to develop a consistent imaging strategy for TAIGER marine seismic reflection data, with particular focus on multiple attenuation. We present one profile from each of three acquisition legs (Fig. 1) to demonstrate some of the challenges multiples impose in crustal-scale imaging, and a strategy for attenuating much of this unwanted energy.

Geologic background

The Taiwan arc-continent collision began 4–7 Ma when buoyant continental crust of the Eurasia plate encountered the Luzon arc of the Philippine Sea plate at the Manila trench (Liu et al. 2001; Suppe 1984; Huang et al. 1997; Lee et al. 2006; Wang 2001). Convergence between the Philippine Sea plate and the Eurasia plate is also accommodated by subduction of South China Sea lithosphere beneath the Philippine Sea plate at the Manila trench south of Taiwan, and by subduction of the Philippine Sea plate beneath the Eurasia plate at the Ryukyu trench east and north of Taiwan (Fig. 1). A convergence rate of 7–8 cm/year in a northwest direction has been well established from GPS data, earthquake focal mechanisms, and global plate models (Chamot-Rooke and Le Pichon 1999; Yu et al. 1997; Hall 2002; Lee and Lawver 1993; Seno et al. 1993). The convergence direction and orientations of the north-trending Luzon arc and northeast-trending Eurasia continental margin created an oblique arc-continent collision, which has led many to view the collision as propagating to the southwest, so that different spatial locations represent different temporal stages of collision (Byrne and Liu 2002; Lee et al. 2006; Suppe 1984).

Southwest of Taiwan, several reflection profiles were acquired in both dip and strike orientations across the Eurasia continental margin. These data extend from the relatively shallow-water continental shelf to intermediate water depths of the continental slope. Geophysical and drilling observations of the Eurasia continental margin in the southwest and central South China Sea have revealed the margin to consist of passive margin sediments overlying moderately extended crust along the continental shelf and transitional crust consisting of highly thinned, volcanically intruded continental crust under the continental slope (Clift et al. 2001; Hayes et al. 1995; Nissen et al. 1995b; Nissen et al. 1995a; Yan et al. 2001; Wang et al. 2006). However, (Hsu et al. 2003) interpreted magnetic anomalies that suggest crust under the lower slope in the vicinity of Taiwan may be volcanically thickened ocean crust, rather than thinned continental crust.

Following rifting of the south China block, the South China Sea opened by seafloor spreading during Oligocene–Miocene (Briais et al. 1993; Taylor and Hayes 1983). Subduction of the South China Sea oceanic lithosphere at the Manila trench beginning in the Miocene created a doubly-vergent accretionary prism, the North Luzon arc and North Luzon forearc basin (Fig. 1). Several profiles were acquired to image these features away from Taiwan where they are not deformed by collision processes and likely represent the initial conditions of the Philippine Sea margin prior to arc-continent collision. The elements of the Manila trench subduction system are also associated with offshore morphologic features of the Taiwan collision. For example, Hengchun Ridge and its emergent equivalent, the Hengchun Peninsula, are the morphologic continuation of the accretionary wedge to the south of Taiwan and the Central Range to the north in Taiwan (Huang et al. 1997). While forearc basin sediments are relatively undeformed in the subduction regime, near Taiwan they are backthrust over the forearc to form the Huatung Ridge (Chi et al. 2003; Lundberg et al. 1997; McIntosh et al. 2005). Onshore, these sediments, as well as the Luzon arc, are further telescoped and obducted to form the Coastal Range along Taiwan's east coast. The TAIGER profiles immediately south of Taiwan were acquired to constrain the deformation of the accretionary prism, Luzon arc, and forearc basin during the initial stages of collision.

While the Philippine Sea plate overrides the Eurasia plate south of Taiwan at the Manila trench, east of Taiwan the Philippine Sea plate subducts northward beneath the Eurasia plate at the Ryukyu trench, where it has generated the Yaeyaema accretionary prism, Hoping and Nanao forearc basins, Ryukyu arc, and Okinawa Trough back-arc basin (Fig. 1). The Ryukyu trench extends north and east from Taiwan, where it predates the Taiwan arc-continent collision. However, the lack of pre-Miocene volcanism in the southwestern Ryukyu arc suggests that this subduction system was not established near Taiwan until the onset of arc-continent collision (Shinjo 1999). Unlike southern and central Taiwan, northern Taiwan is in a state of tension, rather than collision-related compression (Yu et al. 1997; Kao et al. 1998). This has been attributed in varying measures to post-collisional gravitational collapse and the encroachment of the Okinawa Trough or Ryukyu trench (Teng 1996; Kao et al. 1998; Huang et al. 2000; Wang et al. 1999). Additionally, the Luzon arc accreted in the Coastal Range is no longer present north of the Ryukyu trench, suggesting it has been subducted with the Philippine Sea plate or subsided as part of the post-collisional relaxation process. TAIGER data east of Taiwan was acquired to document the accretion and eventual demise of the Luzon arc during arc-continent collision, as well as the complicated dynamic interplay between post-collisional processes, subduction at the Ryukyu trench and back-arc rifting in the Okinawa Trough.

The different seismic transects cover a wide range of water depths that gives rise to both short period and long

period seafloor multiples that may require different approaches to attenuate. Along the continental shelf, short-period multiples may be generated that required gapped deconvolution to effectively attenuate. Techniques such as radon or F–K filtering that rely on velocity discrimination may fail, as the multiples are likely coincident with primary reflections from shallow passive margin strata that may have similar move-out as the multiples. Additionally, shallow reflections typically have lower fold, further limiting the effectiveness of velocity-based methods. However, multiples in deep water have too large of a period for gapped deconvolution to attenuate without damaging primary reflections. In these cases, velocity-based methods may be more effective, as there may be significant difference in move-out between seafloor multiples and the deep crustal reflections they obscure. 2D surface-related multiple elimination (SRME) should in principle attenuate much of the multiple energy regardless of water depth, seafloor relief or lithology. In practice, however, diffracted and out-of-plane multiples often require 3D SRME to attenuate. As seen in previous imaging efforts in the Taiwan region (Berndt and Moore 1999), more than one technique is likely required to effectively attenuate multiples in the TAIGER marine reflection data set.

Data acquisition and processing

Data were acquired during the summer of 2009 with the *R/V Marcus G. Langseth* using a 6-km streamer and 36 air gun source array. The source array consisted of 4 strings of 9 Bolt air guns with a nominal total volume of $\sim$6,600 in^3. Shots were spaced every 50 m, with typical recording length of 15 s. Hydrophones were spaced every 12.5 m, and CDP spacing was 6.25 m. Sources were towed at a depth of 8 m to maximize low frequencies of the source, without sacrificing significant bandwidth. Strong low frequencies in the source are important for imaging reflections from deep crustal structure, which may be low frequency due to the nature of reflecting interface, or because high-frequency energy may not penetrate to the depth of the reflecting interface.

Gapped deconvolution

Standard deterministic gapped deconvolution uses the Weiner-Levinson algorithm (Yilmaz 2001) to design an inverse filter from autocorrelations (or in the multi-channel case, an average of some number of autocorrelations) that will remove the predictable part of the seismic trace (i.e. multiple energy). In practice, gapped deconvolution is used to attenuate short-period seafloor and intra-bed multiples, as well as collapse the source wavelet and sharpen the stacked image. It is often applied to either shot or CDP gathers, in the time–space or tau-p domain. An advantage of gapped deconvolution in tau-p space is that the periodicity of multiples is more consistent for all traces in the gather, as opposed to gathers in the time–space domain where it can vary with offset. An advantage of applying gapped deconvolution to shot gathers is that shot-consistent inverse filters are calculated for each source. In the case of TAIGER reflection data, gapped deconvolution was applied to shot gathers at an early stage in the processing flow, where the major goal is to collapse the source wavelet and gently whiten the amplitude spectrum.

Gapped deconvolution will design an operator from data within a designated window, and then apply that operator to data within another specified window. With the goal of crustal-scale imaging, deconvolution operators must be designed to handle a wavelet that changes with depth due to attenuation. To deconvolve arrivals from shallow sediments and lower-frequency arrivals from deeper crustal levels, a two-window approach was used to compute separate operators for shallow sedimentary and deep crustal arrivals (Figs. 2a, b). Design windows are generally at least 2–3 s long at the near offset, but this may be limited by sedimentary thickness at the window location. It is generally undesirable to include multiples in the design window, but doing so did not appear to significantly degrade the quality of result—likely because multiples contain the same source signature as primary reflections. Similarly, two different application windows must be chosen for the shallow and deep operator (Figs. 2c, d). These are chosen in a similar fashion as the design windows, but with a 600 ms transition zone between the two operators to avoid artifacts.

Our preferred parameters for the shallow window are a 10 ms gap, 164 ms operator length and autocorrelations from 11 traces used to calculate an operator. Preferred parameters used in the deep window are a 32 ms gap, 164 ms operator length and autocorrelations from 11 traces used to calculate an operator. Figure 3 shows an example of gapped deconvolution using the two-window strategy and chosen parameters along the continental slope of the Eurasian margin. For most of the TAIGER data, the source array appears to be effectively tuned, so there is little contamination from a bubble pulse. Because of this, in the sedimentary section (Fig. 3a, b), gapped deconvolution only provides mild whitening of the recorded spectrum. However, deeper crustal reflections (Fig. 3c, d) generally exhibit more ringing. The two-window gapped deconvolution strategy effectively collapses the energy into a single event.

While this strategy is generally successful for most TAIGER reflection data, an exception occurs where strong low-frequency ringing obscures weakly reflective sediments beneath a high-amplitude seafloor reflection (Fig. 4a). The low-frequency ringing may be a result of

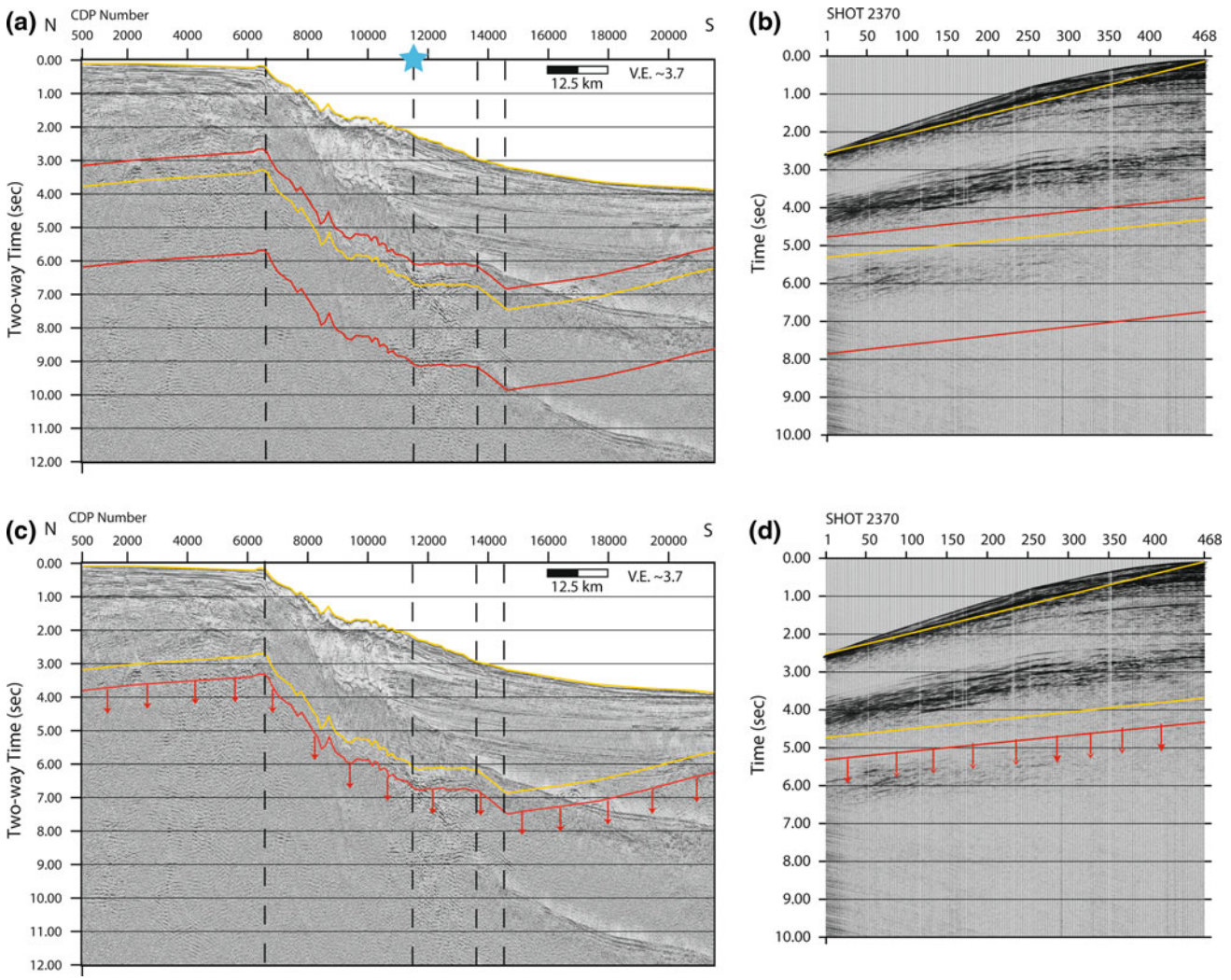

Fig. 2 **a** Profile MGL0905_22 stacked section (see Fig. 1 for location) illustrating arrivals contained within the two design windows for gapped deconvolution. *Yellow line* is the shallow design window encompassing reflections from sedimentary strata, *red line* is the deep design window containing lower frequency, deeper crustal reflections. *Dashed lines* indicate location of window designs. **b** Shot gather, with near offset shifted to the seafloor, illustrating two design windows. Shot location is near CDP 11500 (*blue star*) in (**a**). **c** Stacked section illustrating arrivals shallow (*yellow*) and deep (*red*) operators are applied to. **d** Shot gather, with near offset shifted to the seafloor, illustrating application windows

gun failure during shooting, resulting in a ringing source with an unbalanced spectrum biased towards the low-frequency components. In these cases, deconvolution using any reasonable choice of gap and operator length introduces high-frequency, high-amplitude noise within a single operator length of the seafloor. Averaging over more autocorrelations largely mitigates this problem, though it somewhat dampens the effectiveness of the deconvolution. While the deconvolution is still generally successful at reducing the low-frequency oscillations without introducing any artifacts (Fig. 4b, c), the strongest of these low-frequency oscillations occurs at nearly 0.5 s below the seafloor, and is beyond the ability of gapped deconvolution to reliably attenuate without damaging primary reflections. The reason for such a strong, late oscillation is not entirely clear, but it may be eliminated with a low-cut bandpass filter (Fig. 4d).

2D surface-related multiple elimination (SRME)

2D SRME creates a multiple model based on a series of autoconvolutions of recorded traces (Verschuur et al. 1992). The obvious and oft-stated advantage of SRME is that it does not require any input beyond shot gathers (i.e. seafloor picks or velocities), but rather decomposes input traces into Taylor expansions where each term of the Taylor expansion corresponds to a higher order of multiples. Each Taylor expansion term is computed as a

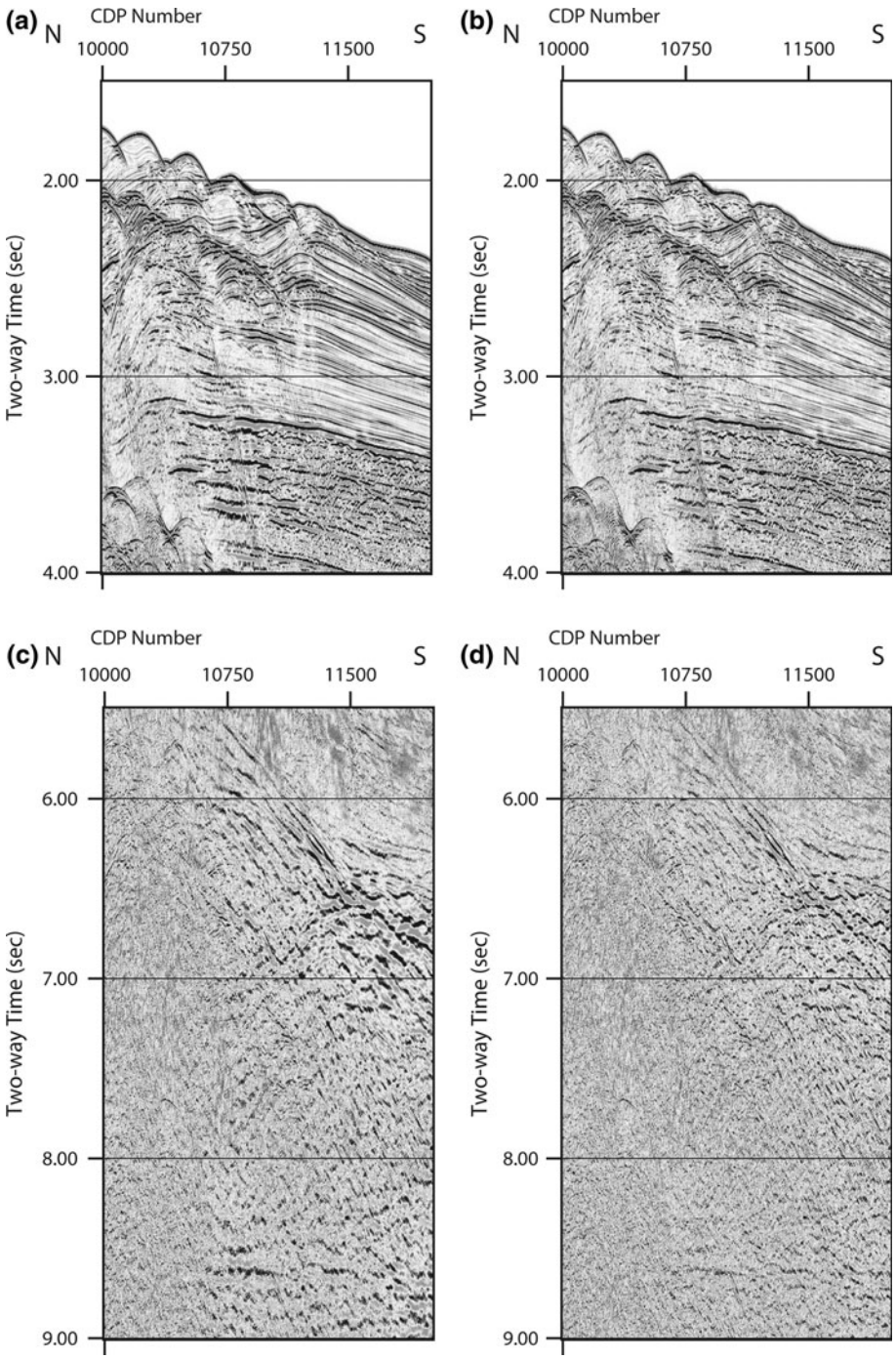

Fig. 3 Stacked section from MGL0905_22 (see Fig. 1 for location) showing continental slope **a** before and **b** after application of shallow gapped deconvolution operators to reflections from the sedimentary section; **c** before and **d** after application of deep gapped deconvolution operators to deep crustal reflections

convolution of input data with itself or lower-order Taylor term. The resultant multiple model may then be adaptively subtracted from the original shot gathers to produce records without multiples.

While 2D SRME does not require a velocity field, it does require a very general 1D RMS velocity to extrapolate from the nearest recorded offset back to true zero offset. Different velocities seem to produce similar quality results, presumably because the difference in hyperbolic curvature from our nearest offset (162.5 m) to zero offset is negligible for different velocities for the frequencies of exploration to crustal scale data. To produce an accurate multiple model, particularly at farther offsets, 2D SRME also requires split-spread geometries, where ray paths are effectively reversed. For marine data, split-spread geometry is simulated by substituting traces from shots coinciding with receiver locations at negative offsets under the assumption of reciprocity. The use of reciprocal shots requires source and receiver spacing to be uniform, so that there exists a source for each receiver location—an

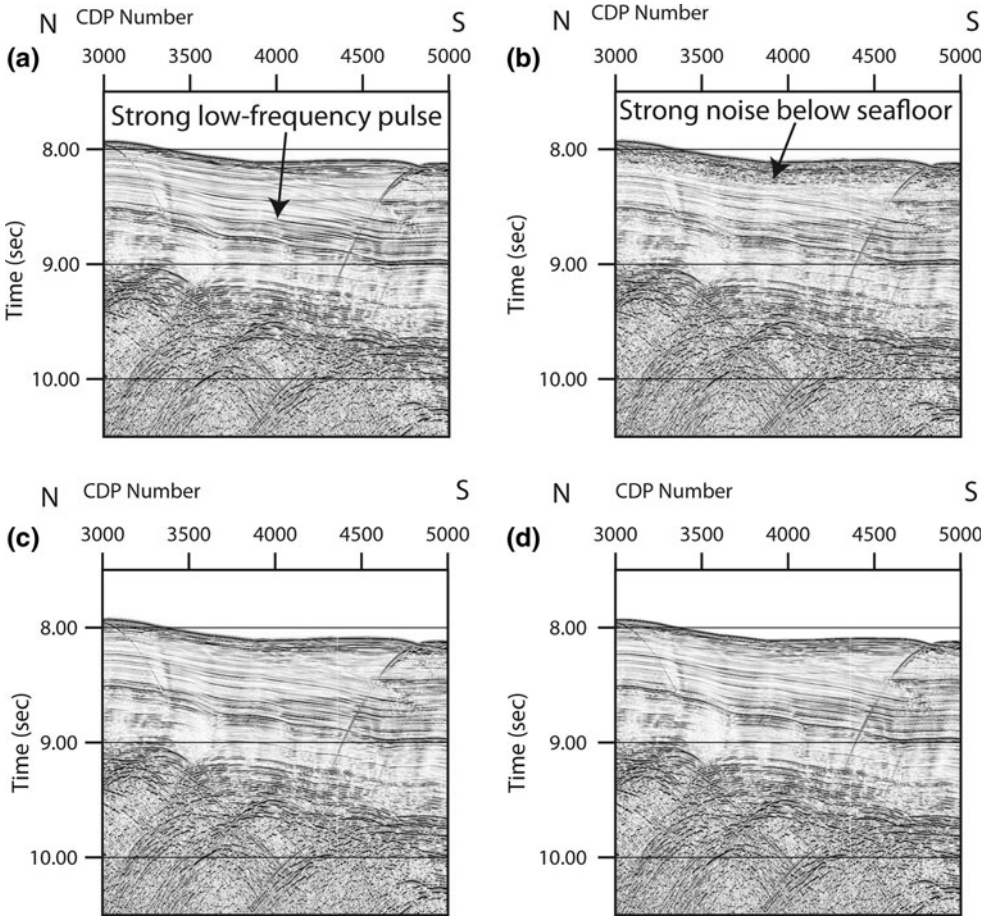

Fig. 4 **a** Stacked section from MGL0906_18N (see Fig. 1 for location) from the Philippine Sea exhibiting strong, low-frequency ringing. **b** Gapped deconvolution with parameters used in Fig. 4 introduces strong noise within one operator length of the seafloor. **c** The problem is mitigated by averaging over a large number of autocorrelations **d** Aggressive low-cut filtering is required to eliminate a strong, low-frequency pulse ~0.5 s below the seafloor

unlikely condition for many reflection data sets. Reciprocal shots must then be generated by either interpolation, or simply copying shot records. This can greatly increase computation time, or potentially degrade the quality of result.

The accuracy of the multiple model generated by 2D SRME depends heavily on these reciprocal traces, particularly at far offsets (Fig. 5). While multiples are attenuated at all offsets, 2D SRME appears to be most successful at the near offsets. For flat sedimentary strata, the strongest multiple energy is contained in the near offsets, so their multiples are effectively attenuated on stacked sections after application of 2D SRME (Fig. 6). Unfortunately, 2D SRME is much less effective for attenuating multiples from more rugose, diffractive basement reflections and areas of high seafloor relief, such as a volcanic edifice or accretionary prism. (Figure 7).

Radon transform multiple attenuation

Radon filtering, unlike 2D SRME, is based on velocity discrimination between primary and multiple reflections, and so requires an earth model. The radon transformation maps seismic energy along specified parabolic trajectories (defined by an NMO velocity or slowness) from NMO-corrected CDP gathers into radon space. Primary events properly flattened with the correct NMO velocity will map along the 0 slowness contour, while multiples, with residual move-out, will map into the positive slowness domain and may be simply muted or filtered out. The ability to transform in and out of radon space with high fidelity, with the ability to separate multiples from primary events, has made radon a standard tool for multiple suppression and random noise attenuation for many years.

Often times, simply transforming into and out of radon space will eliminate much random noise. To attenuate multiples, multiples may be filtered out and the remnant signal transformed back into the time–space domain, or signal may be filtered out and the multiples subtracted from the original input gathers. In practice, the first approach can lead to some loss of seismic character that may be described as appearing "wormy" or "synthetic." The latter approach often produces more desirable results as the signal is unfiltered by the radon process and so retains its original character. Radon filtering, like any velocity-based filter, may create spurious events from random noise. Subtracting multiples from input gathers prevents these artifacts from contaminating subsequent gathers and

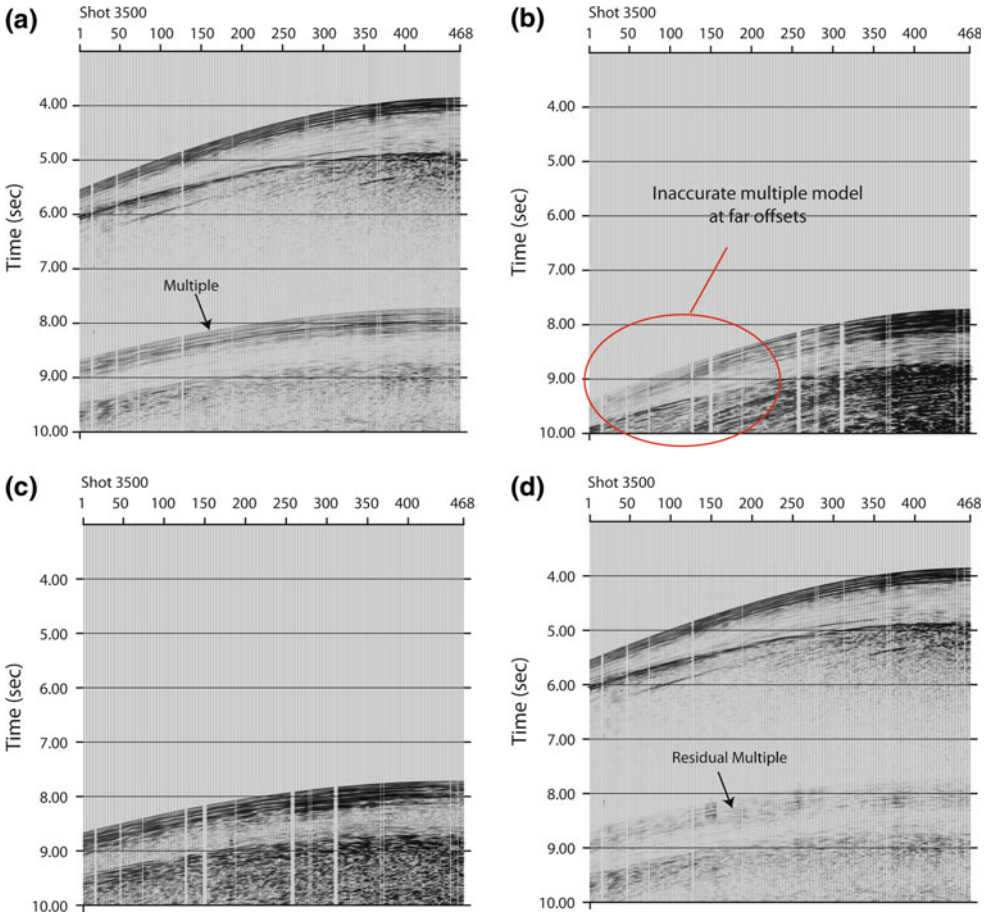

Fig. 5 **a** Shot gather from profile MGL0908_03 before 2D SRME (shot near CDP 20300—see Fig. 1 for profile location, Fig. 6 for location along stacked section) in area of low seafloor relief **b** 2D SRME generates an inaccurate multiple model when only the single input shot gather is used **c** 2D SRME produces a more accurate multiple model when reciprocal traces from adjacent shot gathers are used to simulate a split-spread geometry. Note that model amplitudes do not necessarily reflect those of original shot gathers. Adaptive subtraction or waveform matching is required to effectively attenuate multiples with the modeled multiples. **d** Shot gather after adaptive subtraction of multiple model in **c**. Multiple energy appears to be more effectively attenuated at near offsets than far offsets

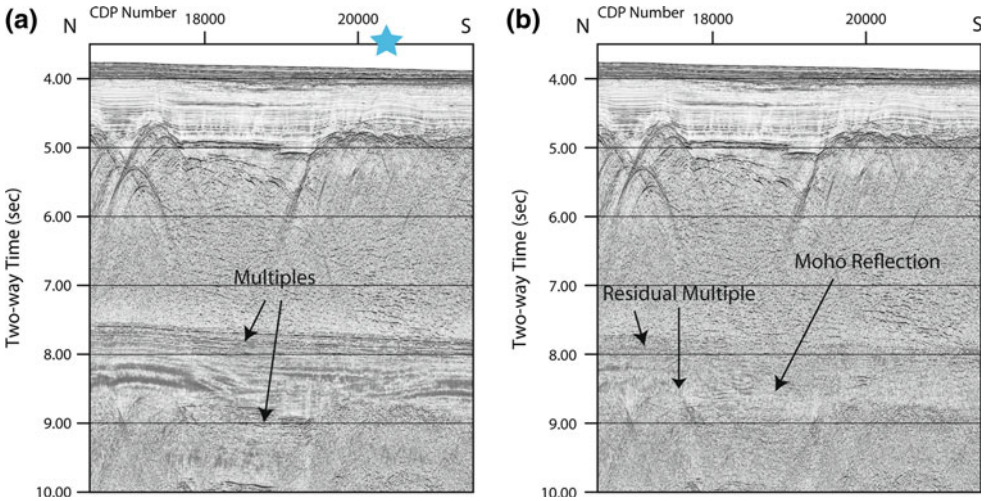

Fig. 6 **a** Stacked section from profile MGL0908_03 before 2D SRME in area of with low seafloor relief (see Fig. 1 for location) **b** Stacked section after 2D SRME. While much of the multiple energy is significantly attenuated, particularly from the flat sediments, significant residual multiple energy remains. *Blue star* is location of shot gather in Fig. 5

stacked sections. However, since multiples may have a wide range of move-out, this approach is more computationally expensive, as a large number of parabolas must be computed for each time sample to represent multiples in radon space.

While radon is generally effective at attenuating multiples, residual multiple energy may still be observed at all offsets (Fig. 8). Figure 8b demonstrates that much of the residual multiple energy is contained at near offsets. This is one of the practical limitations of radon filtering. Energy at near offsets, near the apex of hyperbolic events, will map into the same domain as flattened events (i.e. primary events). Therefore, even after filtering in radon space, multiple energy may not be attenuated at near offsets. This problem may be exacerbated for the low-frequency components of hyperbolic events, as the low frequencies are

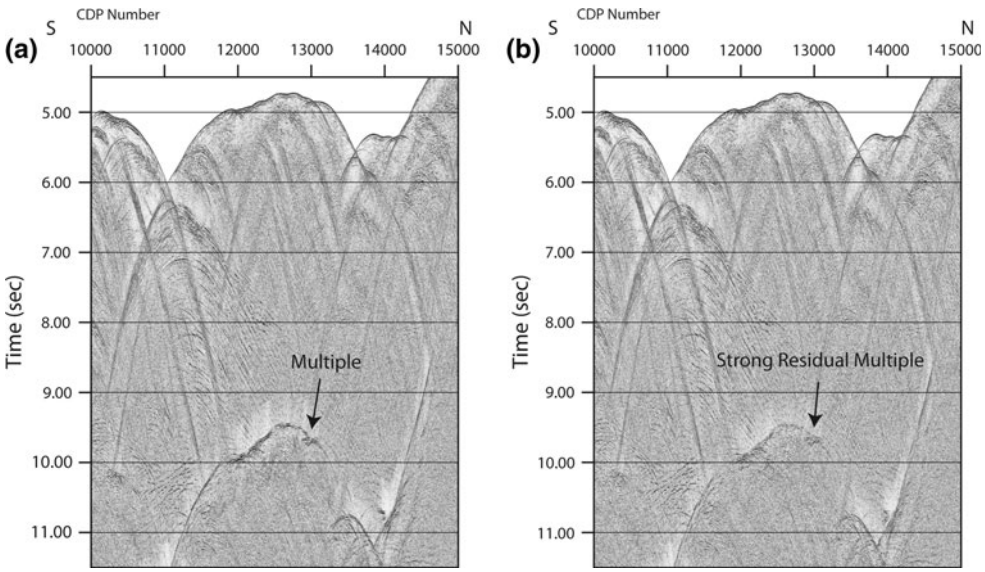

Fig. 7 **a** Stacked section from MGL0906_18N before 2D SRME in accretionary prism with significant seafloor relief (see Fig. 1 for location) **b** Stacked section after 2D SRME. 2D SRME attenuates some multiple energy, but strong residual multiple energy remains

even less sensitive to velocity at near offsets. In some situations, this may lead to a low-frequency residual multiple deep in the crust that may be easily misinterpreted as a deep crust or Moho reflection. Fortunately, the respective limitations of 2D SRME and radon make them highly complementary techniques for attenuating multiples. While radon filtering is ineffective at near offsets but effective for far offsets, 2D SRME is most effective for near offsets and less effective for far offsets (Fig. 8c–f). In the example from MGL0908_03, 2D SRME and radon filtering have greatly attenuated seafloor multiples from flat sedimentary strata and revealed a strong Moho reflector.

Residual multiple attenuation

Any remaining multiple energy at this stage of processing is largely from diffractive, rugose basement or seafloor reflections not attenuated by 2D SRME or radon. For deep water depths where multiples with relatively high dominant frequencies obscure low frequency deep crustal or Moho reflections, an aggressive high-cut bandpass filter may eliminate much of the residual multiple energy (Fig. 9a–d). Additionally, since much of this energy is contained at near offsets, the residual multiple energy may be attenuated by either weighting traces with increasing offset or simply muting the near offsets at the onset of multiple energy. For many of the TAIGER reflection data, we use a simple linear weighting with increasing offset, though more sophisticated schemes may be implemented to optimize signal-to-noise ratio (i.e. (Schoenberger 1996). While trace weighting and inside muting are both computationally inexpensive and produce similar stacked responses (Fig. 9e, f), inside muting has the advantage of being applied to pre-stack gathers at the onset of multiple energy, as opposed to trace weighting, which can potentially degrade the quality of shallower reflections in stacks by enhancing noise at far offsets. However, both techniques prevent multiple energy at near offsets from contaminating the stacked section.

Case study and discussion

Figure 10 shows our processing flow for TAIGER marine reflection data. Minor adjustments may be necessary on a case-by-case basis as data require. Following gapped deconvolution and multiple attenuation as discussed, CDP gathers are pre-stack time migrated using Kirchhoff time migration and then stacked to produce the final image. The stacking velocity field for each profile was transformed into an RMS velocity as an initial velocity field for pre-stack time migration, and refined using residual velocity analysis. In the case of MGL0905_22 and MGL0908_03, only 1–2 iterations of migration and residual analysis were required. However, in the accretionary prism along MGL0906_18N, several iterations were necessary. These profiles are representative of many of the imaging challenges in the TAIGER crustal-scale marine reflection data, and are presented to demonstrate the general success of our processing strategy.

Profile MGL0905_22—Eurasia continental margin shelf and upper slope

Figure 11 shows the pre-stack time migrated image of the Eurasia continental margin along MGL0905_22. This profile extends from water depths of ~150 m along the continental shelf to ~3,000 m down the continental slope.

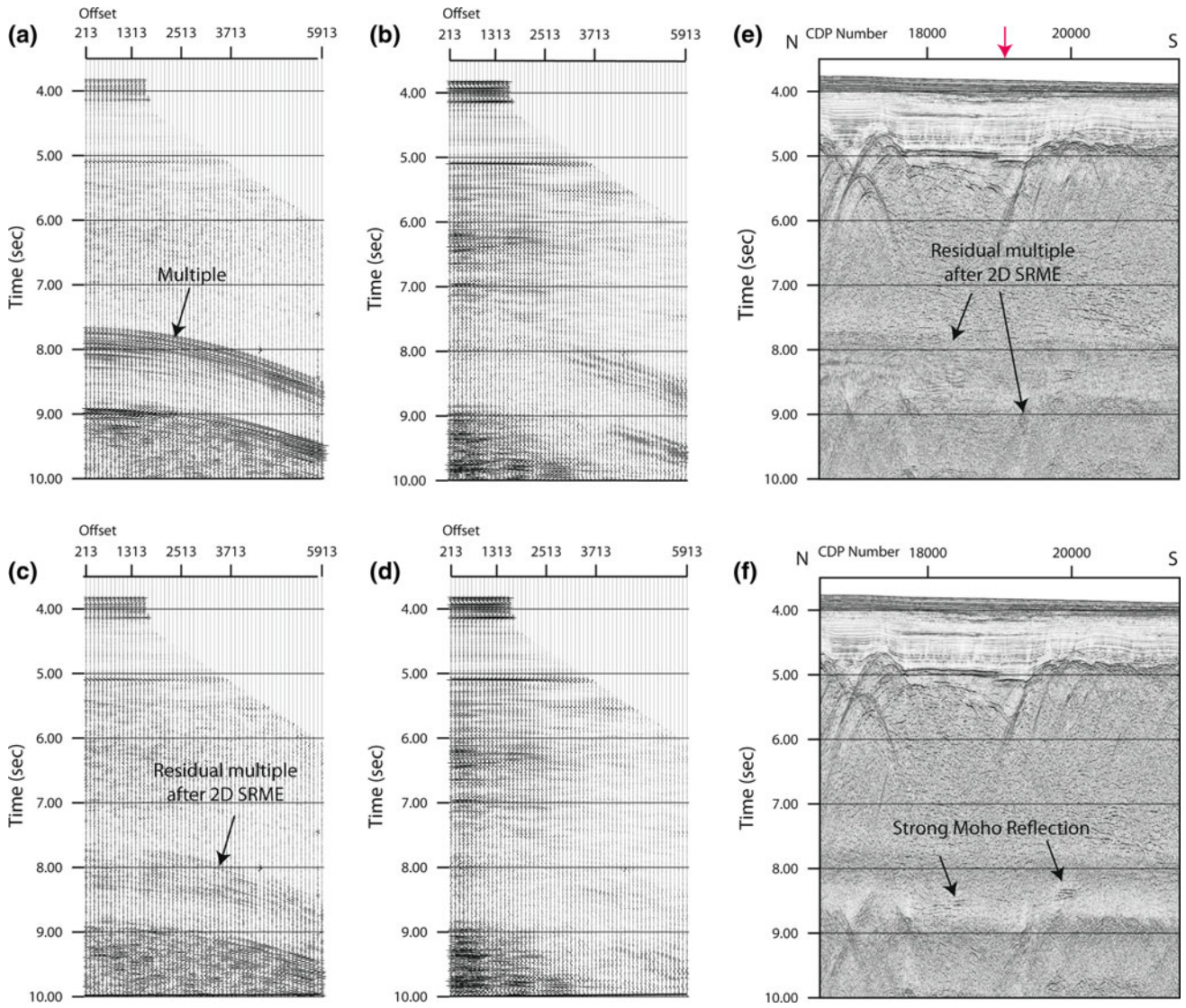

Fig. 8 **a** CDP 19000 from MGL0908_03 NMO-corrected without multiple attenuation **b** CDP after subtraction of multiples from radon filtering. While much of the multiple energy is attenuated, residual multiple energy remains at all offsets. **c** NMO-corrected CDP with 2D SRME result used as input for radon filtering. **d** CDP after both 2D SRME and radon. Multiples are more effectively attenuated at both near and far offsets. **e** Stacked section (MGL0908_03) without radon multiple attenuation (same as Fig. 6b). *Red arrow* is location of CDP in **a**–**d**. **f** Stacked section after radon demultiple. Radon effectively eliminates the residual multiples from sedimentary reflections, but some residual multiple from basement reflections remain

Gapped deconvolution, 2D SRME, and radon filtering effectively suppress multiples along the continental shelf and much of the continental slope. Unfortunately, strong multiple energy persists beneath the upper slope at water depths of ~750–1,500 m. Here, 2D SRME has little effect on multiples, and radon filtering leaves significant multiple energy at near offsets. Multiples here also have similar bandwidth to the sedimentary reflections they obscure. Additionally, stretch muting after NMO-correction reduces the usable offset range at the onset of multiple energy so that offset weighting and inside muting are only marginally effective. While this creates problems in relating sediments of the continental shelf to those down the continental slope, the deeper crustal structure is still observable.

At the continental shelf, these data show about 3 s two-way time (~3–4 km) of foreland basin and post-rift sedimentary strata overlying thick pre-Tertiary basement (Fig. 11a), as expected from extensive exploration seismic and drilling data sets from other sub-basins of the Eurasia margin near Taiwan (Lin et al. 2003; Liu et al. 1997). Extensive normal faulting is also observed that offsets shallow sedimentary strata near the seafloor, as well as the basement reflector at ~3–3.5 s two-way time. Similar normal faulting has been observed in other sub-basins near

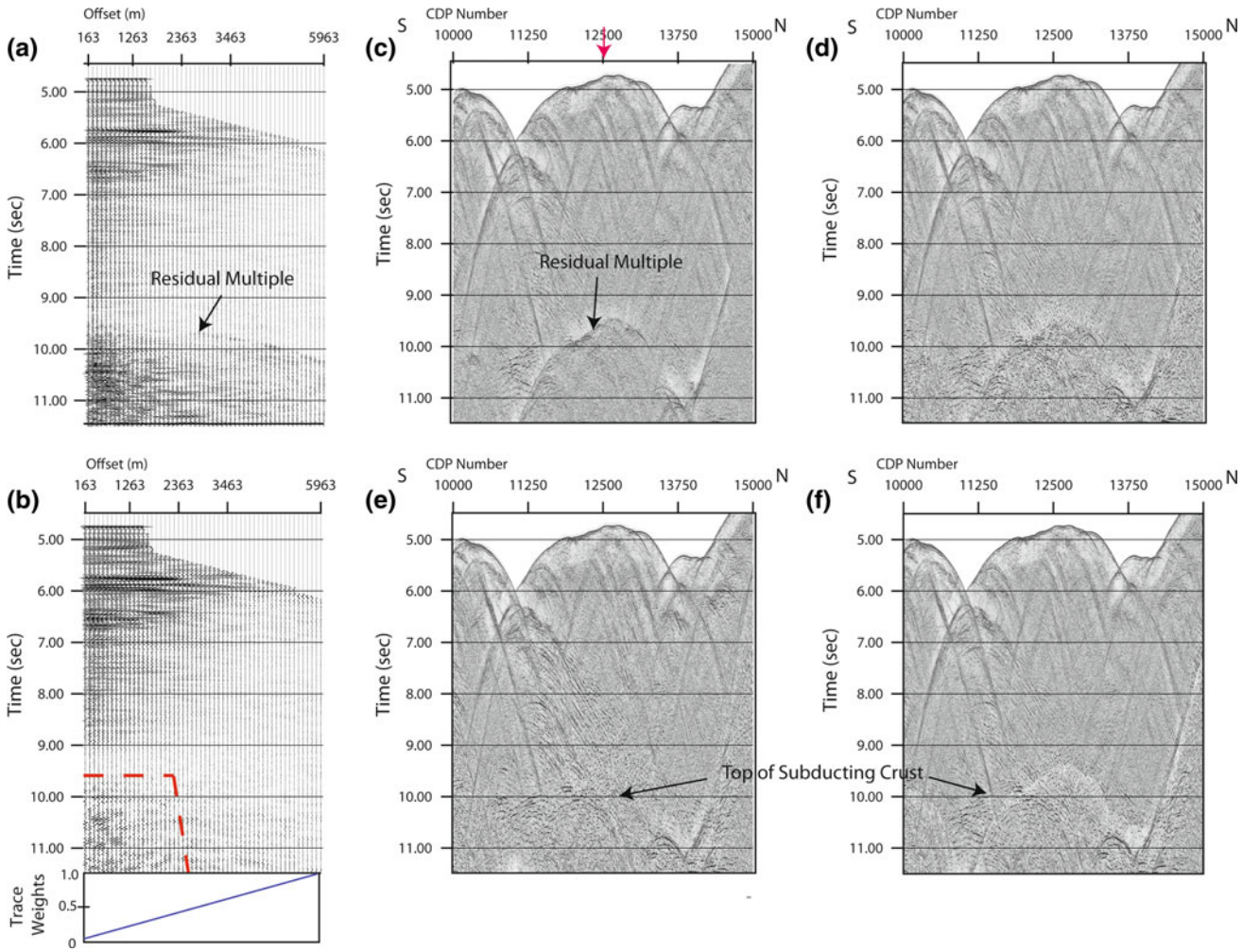

Fig. 9 **a** CDP gather 12500 and **c** stacked section from MGL0906_18N (see Fig. 1 for location) with 2D SRME and radon filtering along the Ryukyu accretionary prism with strong residual multiple energy. *Red arrow* in **c** is location of CDP 12500. **b** CDP gather and **d** stacked section after application of bandpass filter with corners of 2, 5, 20 and 30 Hz. Aggressive bandpass filtering with inside muting (*dashed line* in **b**, stacked section in **e**) or offset-weighted stacking (weights in **b**, stacked section in **f**) attenuate much of the multiple energy 2D SRME and radon filtering do not

Taiwan that has been attributed to prior rifting or more recent collision-induced flexure (Lin and Watts 2002).

While these sedimentary packages and normal faults have been observed in many other data sets near Taiwan, the new TAIGER crustal-scale data reveals significant mid-crustal reflectivity (between ~5 and 7 s two-way time). Additional deep reflectivity may be observed near 10 s two-way time (~25–30 km) that likely represents the Moho discontinuity beneath the continental shelf. While residual multiple energy obscures the strata of the upper slope, this deep Moho reflector is observed to shoal across the upper continental slope, where it is ultimately truncated by a large seaward-dipping normal fault. Unfortunately, the residual multiple energy along the upper slope also obscures the up-dip extent of this crustal-scale normal fault. Across this normal fault, stratigraphic thickness increases to ~4 s two-way time (~5–6 km), and may be separated into an upper package and lower package separated by a relatively high-amplitude reflector interpreted as an unconformity (Yeh et al. 2010). Sediments are much thicker here than at the continental shelf, and our multiple attenuation efforts reveal thin, faulted crustal blocks seaward of the continental shelf (Fig. 11b). While the Moho reflector is not obvious on the crustal block immediately on the down-thrown side of the crustal-scale normal fault, it may be observed rapidly shoaling from 8 to 8.5 s two-way time on the southernmost end of the profile. Locally, crust here is as thin as ~2 s or 5–6 km thick. These crustal blocks are each bounded by normal faults that appear to offset Moho and penetrate into the upper mantle.

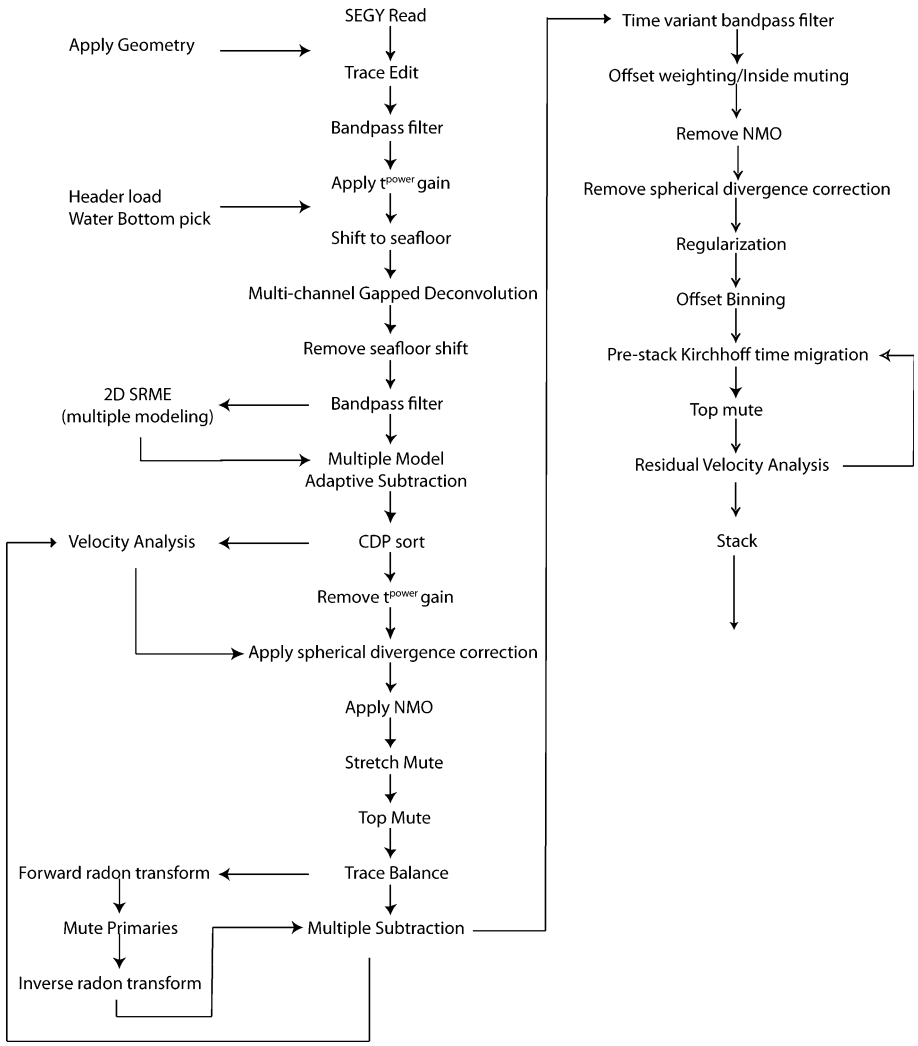

Fig. 10 Processing flow chart for TAIGER marine reflection data through pre-stack time migration

Profile MGL0908_03—lower continental slope and abyssal plane

MGL0908_03 (Fig. 12) continues southward from MGL0905_22 to image the crust beneath the lower continental slope and abyssal plane of the South China Sea near Taiwan. Due to the relatively smooth seafloor topography and intermediate water depths, 2D SRME and radon filtering are successful in attenuating multiples and reveal a strong Moho reflector along much of the profile. The north end of MGL0908_03 overlaps with the south end of MGL0905_22, and so the Moho reflector is observed at ~8 s two-way time, just as seen on the south end of MGL0905_22 (Fig. 12a). The sedimentary section is also observed to be thickest at the north end of MGL0908_03, where crust is thinnest. Two isolated high-amplitude reflectors occur within these post-rift sediments that we interpret as sills, possibly sourced by local magmatic activity associated with extreme crustal thinning observed here.

The Moho reflector deepens to ~10 s two-way time south of this zone, suggesting that the thinnest crust at the south end of MGL0905_22 and north end of MGL0908_03 is a local minimum in crustal thickness. Crust is ~4 s (~11–13 km) thick across the southern extent of MGL0908_03, consistent with regional forward gravity modeling (Yeh and Hsu 2004). While a number of faulted blocks are observed on this profile, they are separated by extensive zones of rugose crust that may be volcanic in nature. Post-rift sediments are much thinner (1–1.5 s two-way time or ~1–2 km thick) over the 11–13 km thick body of crust and generally flat-lying, except where locally disturbed over the crest of volcanic crust. This relationship, as well as the stratigraphic level of sills, would suggest a pulse of post-rift volcanic activity, similar to much of the volcanic activity observed elsewhere in the South China Sea (Yan et al. 2006).

A prominent seamount is imaged at the south end of MGL0908_03 (Fig. 12b). However, just as in the case of the accretionary prism along MGL0906_18N, strong

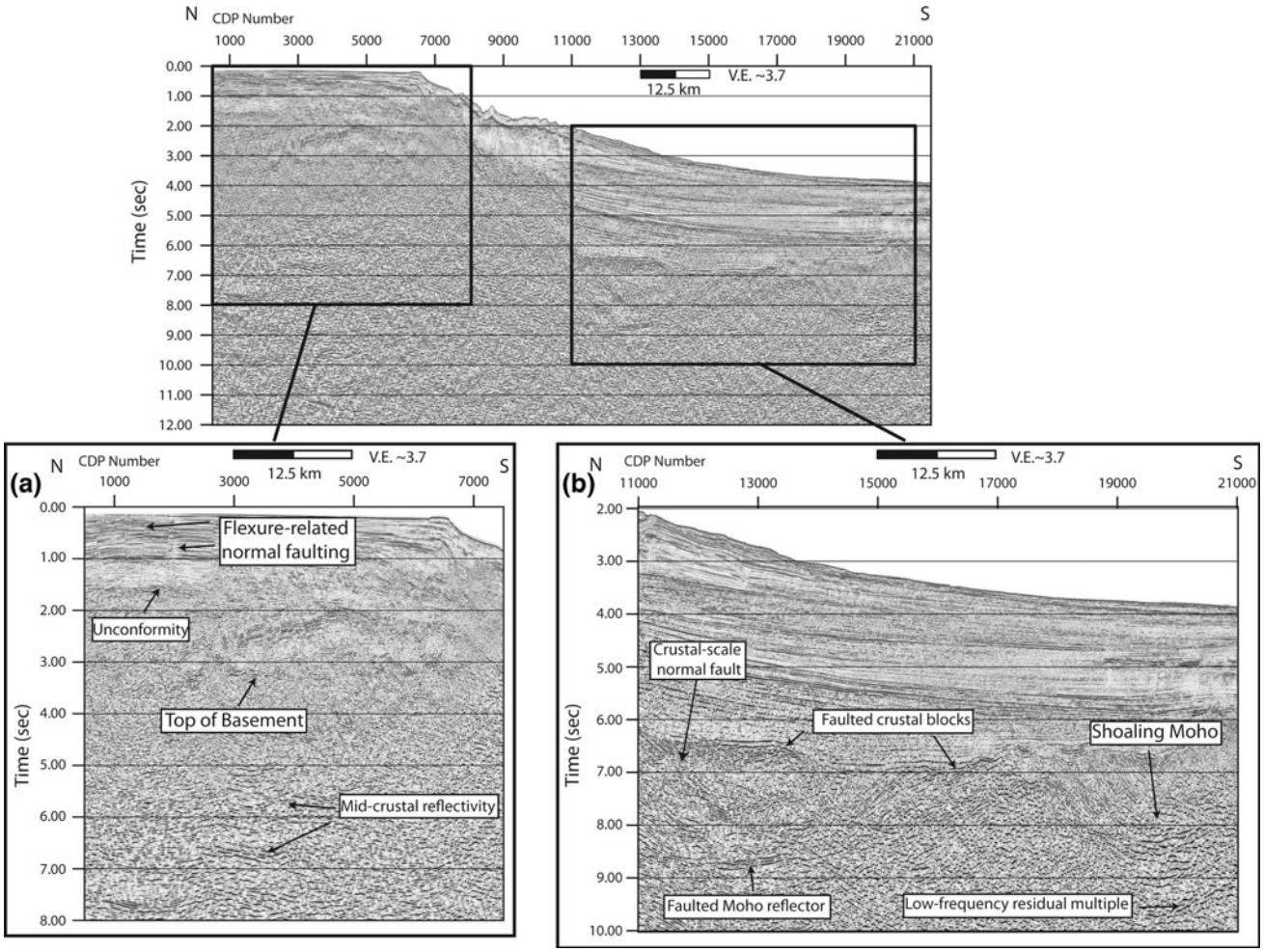

Fig. 11 Profile MGL0905_22 final image of Eurasia continental margin using processing flow in Fig. 10. **a** These data show relatively flat-lying sediments overlying northward dipping strata along the continental shelf. Flexure-related normal faulting offsets basement and shallow strata,. Mid-crustal reflectivity is also observed beneath the shelf. **b** A large crustal-scale normal fault separates thick crust of the continental shelf from thin, normal fault-bound crustal blocks. These faults appear to offset Moho. Crustal thickness is at a minimum at the south end of the line

multiple energy still remains after attempts to attenuate this unwanted energy, although the seamount may not have any internal reflectivity to image. The seamount is apparently flanked by a rotated fault block, which may be pre- or syn-rift sediments deformed during emplacement of the seamount or volcaniclastics from the volcanic seamount. Deformation appears to be more concentrated on the seaward side, where early post-rift sediments are uplifted to the seafloor along the seaward flank of the seamount.

Profile MGL0906_18N—Ryukyu subduction zone

MGL0906_18N (Fig. 13) illustrates the potential for crustal-scale imaging at subduction zones and the processing strategy described in Fig. 10. Although the example is from the Ryukyu subduction zone, similar success is expected for data acquired across the Manila subduction zone. MGL0906_18N was acquired in the deep water (~6,000 m) of the Philippine Sea, so that south of the Ryukyu trench, multiples occur much later in the record than signal from the oceanic crust. South of the trench we observed 1–1.5 s two-way time (1–2 km) of sediments overlying thin oceanic crust (1.5 s two-way time, or ~5 km thick). This observation is consistent with crustal thicknesses previously observed throughout the Philippine Sea east of Gagua ridge (Louden 1980; Murauchi et al. 1968).

Across the Ryukyu trench, the accretionary prism is about 4–7 s (~6–14 km) thick (Fig. 13a). Little internal reflectivity is observed in the accretionary prism away from the trench, either due to lack of significant impedance contrast, or due to strata dipping too steeply to be imaged with the given acquisition geometry. However, several discrete thrusts are imaged, each corresponding to local

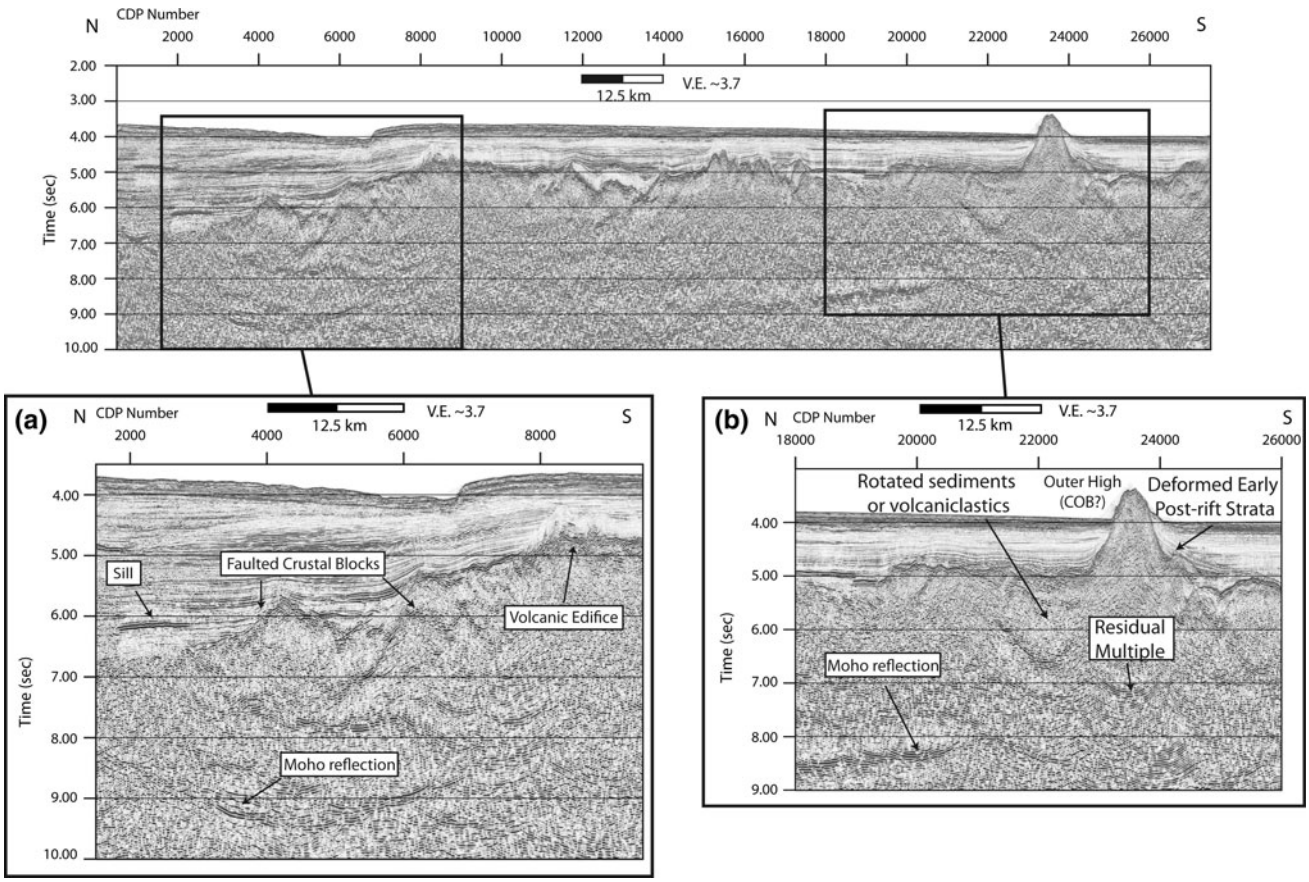

Fig. 12 Profile MGL0908_03 final image in the South China Sea south of Taiwan using processing flow in Fig. 10. **a** Crustal thickness is a minimum at the north end of the line, overlapping with MGL0905_22. Crust is thicker south of this point, and may be characterized as a mix of faulted blocks and volcanic bodies. **b** Crustal structure near prominent seamount south of Taiwan, near a zone of seamounts separating 10–12 km thick crust from normal South China Sea ocean crust to the south (Fig. 1). Seamount is bound by deformed sediment or volcaniclastic packages

bathymetric lows within the accretionary prism. These thrusts extend down to the top of the subducting ocean crust at ~10 s two-way time. Despite some residual multiple energy, the top of the subducting crust is observable beneath much of the accretionary prism.

Along the north end of MGL0906_18N, we image at least four sedimentary packages within the forearc basin (Fig. 13b). The most recent are weakly reflective, flat-lying strata at the basin center. Deeper sediment packages appear to have been folded and possibly faulted as the Philippine Sea Plate subducts beneath. Beneath the forearc basin and crust, multiple attenuation reveals two deep reflectors at 11.5–12 s and 13 s two-way time that may correspond to the forearc Moho and top of subducted crust, respectively. Unfortunately, residual multiple energy makes correlation between these deep reflectors and the top of crust reflector beneath the prism uncertain. Residual multiple energy here also masks the geometry of the forearc backstop at the rear of the accretionary prism. However, reflections from the top of forearc crust, and potentially the forearc Moho, are observable beneath the forearc basin north of this zone of residual multiple energy, but not beneath the prism south of this zone. This suggests that the forearc backstop abruptly terminates within this narrow zone of residual multiples, consistent with previous observations of a steeply-dipping backstop in the southwestern Ryukyu subduction system (Klingelhoefer et al. in press; Font et al. 2000).

Conclusions

The three profiles presented illustrate some of the wide-range of imaging targets and associated challenges in crustal-scale imaging, particularly with respect to multiple contamination. The TAIGER marine reflection data set spans multiple tectonic environments and water depths, so that no one technique suppresses multiples in all environments. However, 2D SRME and radon filtering are highly complementary techniques that effectively suppress much

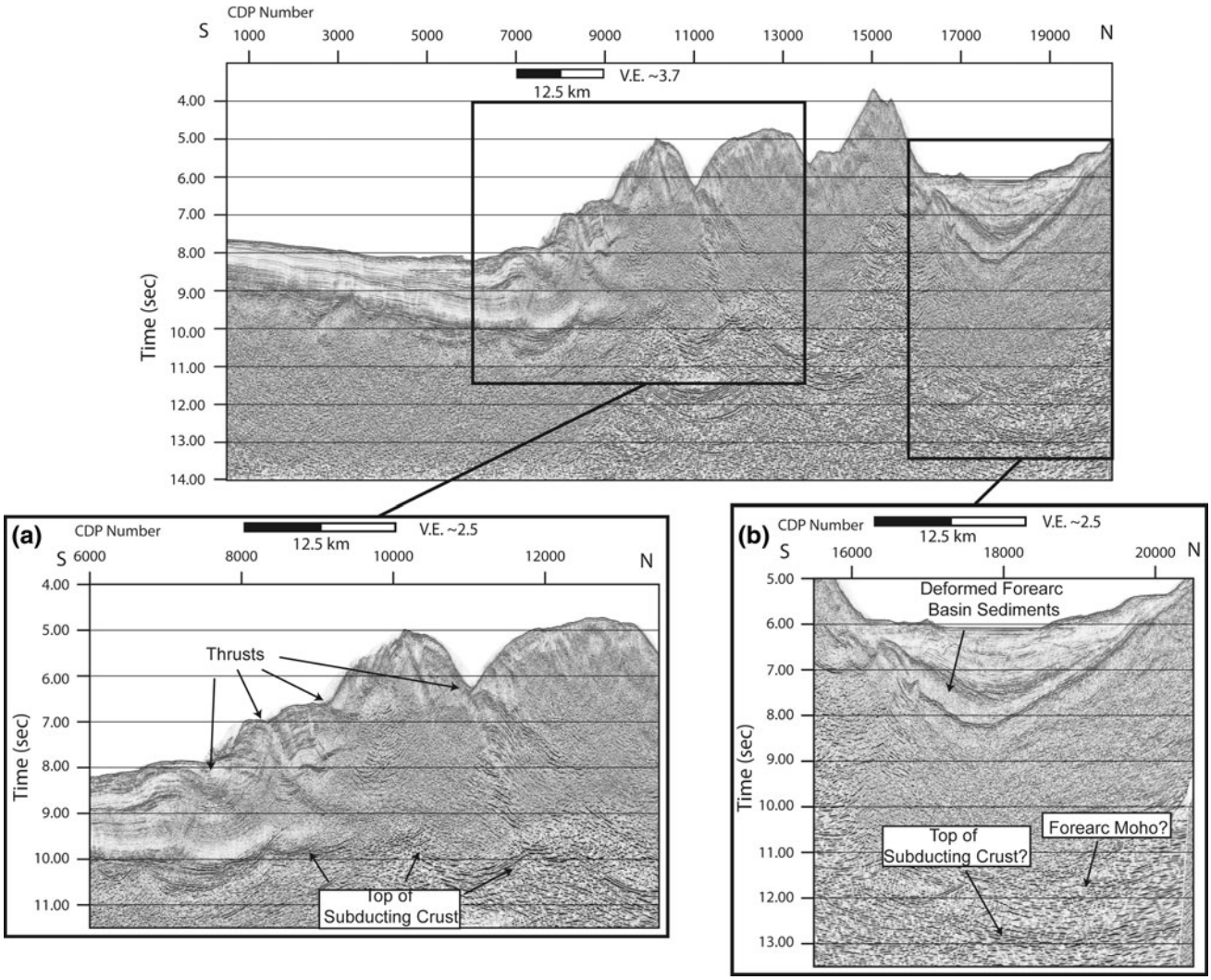

Fig. 13 Profile MGL0906_18N final image across Ryukyu subduction zone using processing flow in Fig. 10. **a** Strata of accretionary prism are either too steep for imaging with these data or non-reflective. Several discrete thrusts are imaged down to the top of subducting ocean crust, which may be observed across much of the prism, despite residual multiple energy. **b** Several distinct sediment packages are observed in the forearc basin, and two deep reflectors are observed beneath forearc crust

of the multiple energy in these environments. Time-variant bandpass filtering and either offset-weighted stacking or inside muting may be used to eliminate much of the residual multiple energy left after 2D SRME and radon filtering.

Multiple attenuation was most successful at intermediate to deep water depths, such as MGL0908_03, where much of the multiple energy comes from relatively flat sediments and obscures a Moho reflector that is of lower-frequency and higher move-out than the multiples. Multiple attenuation was least effective in areas of significant topography such as the accretionary prism along MGL0908_18 N or seamount observed on MGL0908_03. Here, only bandpass filtering and offset-weighting or inside muting attenuate multiple energy with any degree of success.

Although 2D SRME and radon filtering are computationally expensive, MGL0905_22, MGL0908_03, and MGL0906_18N demonstrate some of the potential deep crustal information that may be gained from these multiple attenuation techniques. The imaging strategy discussed reveals that a large, Moho-penetrating crustal-scale normal fault separates thick crust under the continental shelf from thin, normal fault-bound crustal blocks under thick slope deposits. Further to the south, crust is thicker and consists of faulted blocks and possible post-rift volcanic bodies. Across the Ryukyu trench east of Taiwan, our processing flow successfully images deep reflections (forearc Moho and subducting oceanic crust) beneath the accretionary prism. In each case, the presented imaging strategy, with emphasis on multiple attenuation, results in high-quality

crustal-scale images that provide important constraints on the dynamic processes in the vicinity of Taiwan.

Acknowledgments The results of this paper would not be possible without the superior facilities of the *R/V Marcus G. Langseth*, and the hard work of the captain, crew and science staff. We would like to thank the many Taiwanese researchers and students involved in the TAIGER project, including (but not limited to), Dr. Chao-Shing Lee, Dr. Shu-Kun Hsu, Dr. T.K. Wang, and Dr. Char-Shine Liu, who also provided many useful suggestions in the preparation of this manuscript. We would also like to thank the three anonymous reviewers for their insightful feedback. Data were processed with Paradigm's Focus and Geodepth software. Figures were made using Focus and GMT. This research was made possible through the NSF Continental Dynamics program (Grant EAR-0408609) and support from Taiwan's National Science Council, Central Geologic Survey, and Ministry of Interior. University of Texas Institute for Geophysics contribution #2462.

References

Berndt C, Moore GF (1999) Dependence of multiple-attenuation techniques on the geologic setting: a case study from offshore Taiwan. Lead Edge 18:74–80

Briais A, Patriat P, Tapponnier P (1993) Updated Interpretation of Magnetic Anomalies and Seafloor Spreading Stages in the South China Sea: Implications for the Tertiary Tectonics of Southeast Asia. J Geophys Res 98(B4):6299–6328

Byrne TB, Liu C-S (2002) Preface: Introduction to the geology and geophysics of Taiwan. In: Byrne TB, Liu C-S (eds) Geology and geophysics of an Arc-continent collision, Taiwan, vol 358. The geological society of America, pp i–iv

Chamot-Rooke N, Le Pichon X (1999) GPS determined eastward Sundaland motion with respect to Eurasia, confirmed by earthquakes slip vectors at Sunda and Philippine trenches. Earth Planet Sci Lett 173:439–455

Chi W-C, Reed DL, Moore G, Nguyen T, Liu C-S, Lundberg N (2003) Tectonic wedging along the rear of the offshore Taiwan accretionary prism. Tectonophysics 374:199–217

Clift PD, Lin J, Party OLS (2001) Patterns of extension and magmatism along the continent-ocean boundary. Geological Society of London Special Publication, South China Margin

Davis D, Suppe J, Dahlen FA (1983) Mechanics of fold-and-thrust belts and accretionary wedges. J Geophys Res 88(B2):1153–1172

Font Y, Liu C-S, Schnurle P, Lallemand S (2000) Constraints on backstop geometry of the southwest Ryukyu subduction based on reflection seismic data. Tectonophysics 333:135–158

Hall R (2002) Cenozoic geological and plate tectonic evolution of SE Asia and the SW Pacific: computer-based reconstructions, model and animations. J Asian Earth Sci 20:353–431

Hayes DE, Nissen SS, Buhl P, Diebold J, Bochu Y, Weijun Z, Yongqin C (1995) Throughgoing crustal faults along the northern margin of the South China Sea and their role in crustal extension. J Geophys Res 100(11):22435–22446

Hsu S-K, Yeh Y-C, Doo W-B, Tsai C-H (2003) New bathymetry and magnetic lineations identifications in the northernmost South China Sea and their tectonic implications. Mar Geophys Res 25:29–44

Huang C-Y, Wu W-Y, Chang C-P, Tsao S, Yuan PB, Lin C-W, Kuan-Yuan X (1997) Tectonic evolution of accretionary prism in the arc-continent collision terrane of Taiwan. Tectonophysics 281:31–51

Huang C-Y, Yuan PB, Lin C-W, Wang TK, Chang C-P (2000) Geodynamic processes of Taiwan arc-continent collision and comparison with analogs in Timor, Papua New Guinea, Urals and Corsica. Tectonophysics 325:1–21

Kao H, Shen Sern-su J, Ma K-F (1998) Transition from oblique subduction to collision: Earthquakes in the southernmost Ryukyu arc-Taiwan region. J Geophys Res 103(B4):7211–7229

Klingelhoefer F, Berthet T, Lallemand S, Schnurle P, Lee C-S, Liu C-S, McIntosh K, Theunissen T (*In Press*) Velocity structure of the southern Ryukyu margin east of Taiwan: results from the ACTS wide-angle seismic experiment. Tectonophysics

Lee T-Y, Lawver LA (1993) Cenozoic plate reconstruction of the South China Sea region. Tectonophysics 235:149–180

Lee Y-H, Chen C–C, Liu T-K, Ho H-C, Lu H-Y, Lo W (2006) Mountain building mechanisms in the Southern Central Range of the Taiwan Orogenic Belt: from accretionary wedge deformation to arc-continental collision. Earth Planet Sci Lett 252:413–422

Lin AT, Watts AB (2002) Origin of the West Taiwan basin by orogenic loading and flexure of a rifted continental margin. J Geophys Res 107 (B9), 2185

Lin AT, Watts AB, Hesselbo SP (2003) Cenozoic stratigraphy and subsidence history of the South China Sea margin in the Taiwan region. Basin Res 15:453–478

Liu C-S, Huang IL, Teng LS (1997) Structural features off southwestern Taiwan. Mar Geol 137:305–319

Liu T-K, Hsieh S, Chen Y-G, Chen W-S (2001) Thermo-kinematic evolution of the Taiwan oblique-collision mountain belt as revealed by zircon fission track dating. Earth Planet Sci Lett 186:45–56

Louden KE (1980) The crustal and lithospheric thicknesses of the Philippine Sea as compared to the Pacific. Earth Planet Sci Lett 50:275–288

Lundberg N, Reed DL, Liu C-S, Jay Lieske J (1997) Forearc-basin closure and arc accretion in the submarine suture zone south of Taiwan. Tectonophysics 274:5–23

McIntosh K, Nakamura Y, Wang T-K, Shih R-C, Chen A, Liu C-S (2005) Crustal-scale seismic profiles across Taiwan and western Philippine Sea. Tectonophysics 401:23–54

Murauchi S, Den N, Asano S, Hotta H, Yoshii T, Asanuma T, Hagiwara K, Ichikawa K, Sato T, Ludwig WJ, Ewing JI, Edgar NT, Houtz RE (1968) Crustal structure of the Philippine Sea. J Geophys Res 73(10):3143–3171

Nissen SS, Hayes DE, Bochu Y, Weijun Z, Yongqin C, Xiaupin N (1995a) Gravity, heat flow, and seismic constraints on the processes of crustal extension: Northern margin of the South China Sea. Journal of Geophysical Research 100(11):22447–22483

Nissen SS, Hayes DE, Buhl P, Diebold J, Bochu Y, Weijun Z, Yongqin C (1995b) Deep penetration seismic soundings across the northern margin of the South China Sea. Journal of Geophysical Research 100(11):22407–22433

Schoenberger M (1996) Optimum weighted staack for multiple suppresion. Geophysics 61(3):891–901

Seno T, Stein S, Gripp AE (1993) A model for the motion of the Philippine Sea plate consistent with NUVEL-1 and geological data. J Geophys Res 98(B10):17941–17948

Shinjo R (1999) Geochemistry of high Mg andesites and the tectonic evolution of the Okinawa Trough-Ryukyu arc system. Chem Geol 157:69–88

Suppe J (1984) Kinematics of arc-continent collision, flipping of subduction, and back-arc spreading near Taiwan. Mem Geol Soc China 6:21–33

Taylor B, Hayes D (1983) Origin and history of the south China Sea Basin. In: The tectonic and geologic evolution of Southeast Asian Seas and Islands, Part 2, vol AGU geophysical monogram 27. pp 23–56

Teng LS (1996) Extensional collapse of the northern Taiwan mountain belt. Geology 24(10):949–952

Verschuur DJ, Berkhoust AJ, Wapenaar CPA (1992) Adaptive surface-related multiple elimination. Geophysics 57(9):1166–1177

Wang W-H (2001) Lithospheric flexure under a critically tapered mountain belt: a new technique to study the evolution of the Tertiary Taiwan orogeny. Earth Planet Sci Lett 192:571–581

Wang K-L, Chung S-L, Chen C-H, Shinjo R, Yang TF, Chen C-H (1999) Post-collisional magmatism around northern Taiwan and its relation with opening of the Okinawa Trough. Tectonophysics 308:363–376

Wang TK, Chen M-K, Lee C-S, Xia K (2006) Seismic imaging of the transitional crust across the northeastern margin of the South China Sea. Tectonophysics 412:237–254

Wu FT, Rau R-J, Salzberg D (1997) Taiwan orogeny: thin-skinned or lithospheric collision? Tectonophysics 274:191–220

Yan P, Di Z, Zhaoshu L (2001) A crustal structure profile across the northern continental margin of the South China Sea. Tectonophysics 338:1–21

Yan P, Deng H, Liu H, Zhang Z, Jiang Y (2006) The temporal and spatial distribution of volcanism in the South China Sea region. J Asian Earth Sci 27:647–659

Yeh Y-C, Hsu S-K (2004) Crustal structures of the northernmost South China Sea: Seismic reflection and gravity modeling. Mar Geophys Res 25:45–61

Yeh Y-C, Sibuet J-C, Hsu S-K, Liu C-S (2010) Tectonic evolution of the Northeastern South China Sea from seismic interpretation. J Geophys Res 115

Yilmaz O (2001) Seismic data analysis, 2nd edn. Society of Exploration Geophysics, Tulsa

Yu S-B, Chen H-Y, Kuo L-C (1997) Velocity field of GPS stations in the Taiwan area. Tectonophysics 274:41–59